JOURNAL OF MATERIALS SCIENCE 29 (1994) 239–249

Strengthening potential of the cubic σ precipitate in Al–Cu–Mg–Si alloys

R. D. SCHUELLER*, F. E. WAWNER
Department of Materials Science and Engineering, University of Virginia, Charlottesville, VA 22903, USA

A. K. SACHDEV
Metallurgy Department, GM Research Labs, Warren, MI 48090, USA

An interesting cubic-shaped precipitate was observed in the matrix of a squeeze-cast Al–4.3 wt% Cu–2.0 wt% Mg/SiC composite which was heat-treated to a T7 condition. Although this phase had been observed by a few investigators in the past, it had never been examined in detail until now. This cubic phase generally had an edge length ranging from 30 to 50 nm and existed in volume fractions as high as 3.8%. Theoretical strengthening models predicted this phase to have good potential for precipitate strengthening. In addition, the cubic phase exhibited a low rate of coarsening at temperatures as high as 250 °C; apparently due to its low interfacial energy. Consequently, this cubic precipitate shows potential for increasing the useful temperature range of aluminium alloys and composites and could be of great importance to the aerospace and automotive industries.

1. Introduction

A need exists for an aluminium alloy or aluminium-matrix composite with stable elevated-temperature properties. Currently available high-strength aluminium alloys soften after a long period of exposure to elevated temperatures due to coarsening of the precipitates designed to strengthen them. Dislocations easily bypass these coarsened precipitates, resulting in a loss of mechanical properties. Of the available aluminium alloys, S′ (Al_2CuMg)-strengthened Al–Cu–Mg alloys have demonstrated the best strength retention after long periods at temperatures of 130–140 °C [1]. Thus it was an Al–2.2Cu–1.5Mg–1Fe–1Ni–0.2Si alloy that was used for the skin of the supersonic Concorde where such temperatures are encountered. However, S′ coarsens significantly at temperatures greater than 150 °C causing loss of mechanical properties. Therefore to extend the useful temperature range of aluminium alloys a precipitate-strengthening phase is required which is coarsening-resistant at temperatures greater than 150 °C.

Relatively high values of specific strength (strength/density) and specific modulus (modulus/density) make aluminium alloys and aluminium-matrix composites very appealing to the aerospace and automotive industries. If these materials could be made to withstand higher temperatures they could, for example, be used as wing skins in the high-speed civil transport plane where they would be exposed to temperatures near 170 °C for 120 000 h. Thus they could replace heavier and more expensive titanium alloys in many aerospace applications. Heat-resistant aluminium alloys would also be useful in replacing heavy iron components such as pistons or piston rods in automobile engines where temperatures can reach as high as 250 °C.

In the examination of a heat-treated Al–4.3Cu–2Mg/SiC whisker composite, an unusual cubic-shaped precipitate was observed. Although this phase had been observed by a few investigators in the past [1–3], it had never been identified or examined in detail. A recent paper by the current authors [4] utilized electron diffraction patterns, X-ray analysis techniques and computer modelling to identify the phase as $Al_5Cu_6Mg_2$, a phase not previously known to exist in aluminium-rich alloys. For simplicity the cubic precipitate was designated σ. The σ phase has a cubic crystal structure with a lattice parameter of 0.831 nm. This phase has the simple orientation relationship $\langle 100\rangle_\sigma \| \langle 100\rangle_m$ and $\{100\}_\sigma \| \{100\}_m$. Samson [5] had shown $Al_5Cu_6Mg_2$ to be in the space group Pm3 with 39 atoms per unit cell. The present paper will discuss the potential of the σ phase for precipitate-strengthening at ambient and elevated temperatures.

2. Experimental procedure

2.1. Sample preparation

The composite samples were prepared for examination with the transmission electron microscope (TEM) in the following manner: material was polished to a thickness of 100 μm at which time 3 mm discs were punched out and further polished to a thickness of 20 μm. The final thinning was performed using a Gatan ion mill equipped with a liquid nitrogen cold stage. A voltage of 4 kV and an initial angle of 20° was used until perforation. The samples were then further milled for 1–2 h at an angle of 10°. Unreinforced

* *Present address*: Electronic Products Division, 3M Center, Austin, TX 78769, USA

samples were electropolished with a 3:1 methanol: nitric acid solution at 10 V, 1.2 A and −20 °C. Samples were stored in a vacuum desiccator prior to TEM analysis.

Samples were examined using a Philips EM 400 TEM equipped with a double tilt holder and a single tilt *in situ* hot stage holder at an accelerating voltage of 120 kV. Energy-dispersive X-ray spectroscopy (EDXS) capabilities were also utilized.

3. Results and discussion

3.1. The S′ phase

Al–Cu–Mg alloys with a Cu:Mg ratio in the range 1.5:1 to 4:1 are strengthened primarily by the equilibrium S′ phase (Al_2CuMg) [6–8]. This phase is seen as thin rods or needles oriented along ⟨0 0 1⟩ directions and can be identified by characteristic ⟨0 2 1⟩ streaks in the $\mathbf{B} = \{1\,1\,2\}$ diffraction pattern.

S′ is the phase most heavily depended on for strengthening in 2*xxx* series alloys. The critical rod diameter, above which precipitate shearing does not take place, has been determined to be approximately 2.0 nm [9]. At peak strengthening the S′ phase results in an impressive increase in yield strength of nearly 275 MPa (40 ksi) [10] (this value was obtained by comparing the yield strengths of the peak-aged and overaged material). Some problems with S′ are that (i) the rapid heterogeneous nucleation of S′ on dislocations can result in an inhomogeneous distribution (and precipitate-free zones also develop near the dislocations); and (ii) the S′ phase coarsens above temperatures of 150 °C, causing a loss of mechanical properties.

3.2. Microstructural observations

Although S′ was the only expected precipitate phase in the Al–4.3Cu–2Mg matrix, three other phases were also commonly observed: θ′ (Al_2Cu), a plate-shaped phase typically observed in Al–Cu alloys, β (Mg_2Si) a rod-shaped phase usually found in Al–Mg–Si alloys, and the cubic σ phase. The σ phase is known to nucleate in Al–Cu–Mg alloys after the addition of small amounts of Si (0.2–0.5 wt %) [1–3]. However, the mechanism by which Si causes nucleation is unknown and is discussed in a companion paper [11]. The cubic-shaped σ phase typically ranged in size from 30–50 nm and was measured in volume fractions as high as 3.8%, as shown in Fig. 1. This was the maximum possible volume fraction of the σ phase in the Al–4.3Cu–2Mg matrix and was limited by the Cu content. On a local scale the σ phase was distributed in a homogeneous manner, suggesting it may be a good precipitation-hardening phase. However, up to this point there has been no success in nucleating the σ phase uniformly throughout a bulk specimen (primarily due to the segregation effects of Si, also discussed elsewhere) [11]. Therefore mechanical tests could not be performed which would directly indicate the strengthening contribution of this phase. As a result, a detailed theoretical approach was required to estimate the potential of this phase for precipitate strengthening.

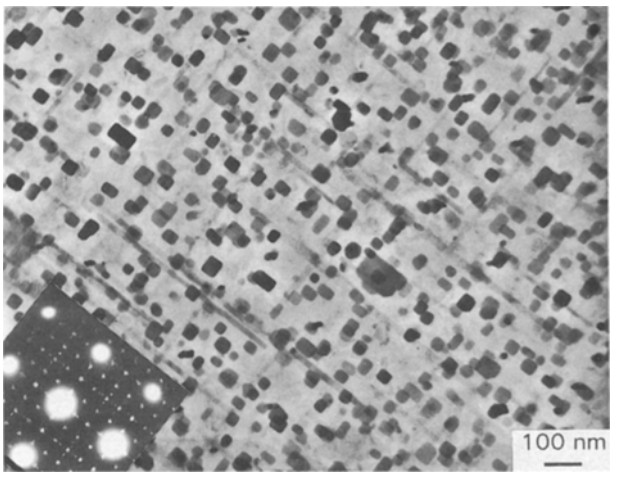

Figure 1 A high concentration of the cubic σ phase, measured to be approximately 3.8 volume fraction. Near $\mathbf{B} = \langle 0\,0\,1 \rangle$.

3.3. Precipitate-strengthening mechanisms

Precipitate strengthening is one of the most effective methods of increasing the yield strength of aluminium alloys. Precipitates harden a material by impeding the motion of dislocations within it. Due to the microstructural characteristics of the cubic σ phase, this phase will interact with dislocations through three main mechanisms: (i) coherency hardening, (ii) order hardening and (iii) modulus hardening. Some of these mechanisms may also act together simultaneously to repel dislocations. The amount of force exerted by the particle on an approaching dislocation will determine whether the dislocation shears the precipitate or bypasses it. It is well known that small precipitates are generally prone to shearing. However, as precipitates grow to a critical size their strength becomes great enough to prevent dislocations from cutting through them. When precipitates grow larger the dislocations are instead forced to bypass them either by looping, cross-slipping or climbing. In the present paper particle looping by the Orowan process will be assumed, since analysis by this process is more straightforward and gives an upper bound for strengthening. The peak strength of an alloy usually occurs at the critical particle size d_c, the point where precipitate shearing gives way to Orowan looping.

3.4. Coherency hardening

Coherency hardening arises from elastic strain at the interface with a particle which is not perfectly coherent with the matrix. This elastic strain interacts with the strain field of nearby dislocations, causing some dislocations to be attracted and some to be repelled, depending on the orientation of their Burgers vector. To quantify the maximum force exerted on a dislocation an equation is provided by Ardell [12] for the misfit parameter of a spherical coherent particle:

$$\varepsilon = \delta\left(1 + \frac{2G_m(1 - 2\nu)}{G_p(1 + \nu)}\right) \quad (1)$$

where ν is Poisson's ratio for the particle, G_m and G_p are the shear modulus for the matrix and the particle respectively, and δ is the misfit between the phases

given by

$$\delta = \frac{d_1 - d_2}{(1/2)(d_1 + d_2)} \quad (2)$$

where d_1 and d_2 are the planar spacings in the matrix and precipitate, respectively. The coherency force exerted on a dislocation increases as it approaches the particle. The force becomes a maximum at the particle–matrix interface, and for an edge dislocation has been estimated by Gerold *et al.* [13] (using isotropic elasticity theory) to be

$$F = 2G_m \varepsilon b d \quad (3)$$

where b is the length of the Burgers vector, d the particle diameter and ε the misfit parameter defined above. Since $F = Gb^2$ at the start of looping [14] the critical particle size from coherency strengthening can be written

$$d_c = b/2\varepsilon \quad (4)$$

The elastic misfit between the planes of the σ phase ($d_{400} = 0.20775$ nm) and the aluminium matrix ($d_{200} = 0.202$ nm) is 2.8%. Evidence of this elastic strain at the particle–matrix interface is revealed by strain lobes (contrast differences caused by the bending of aluminium planes), as shown in Fig. 2. The fact that these strain lobes only exist in the matrix implies that the shear modulus of the matrix is much lower than that of the σ phase.

To calculate the misfit parameter of σ (given by Equation 1), an estimate for the shear modulus of the σ phase must first be obtained. Since the σ phase ($Al_5Cu_6Mg_2$) is nearly half Cu and half Al, it stands to reason that the shear modulus of the phase likely lies somewhere between the values for Al (28 GPa) and Cu (47 GPa). The shear modulus of the θ phase (Al_2Cu), which is only one-third Cu, has been determined to be 36 GPa [15]. The S′ phase (Al_2CuMg) has been estimated to have a shear modulus of 44 GPa [9]. The σ phase, which is nearly half Cu, would consequently be expected to have a higher modulus than θ or S′.

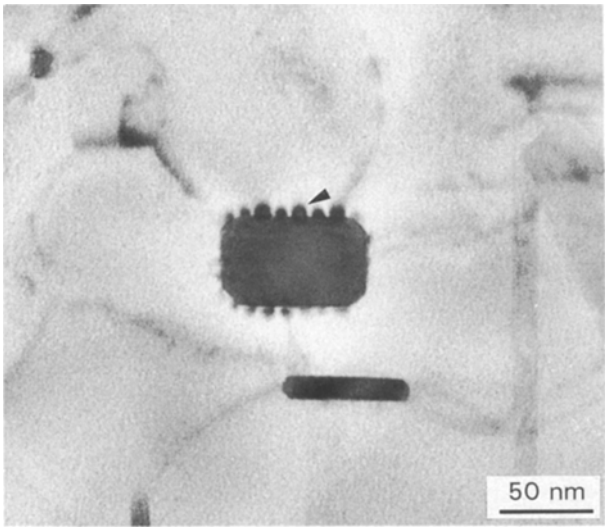

Figure 2 Strain lobes commonly observed at the interface of the σ phase.

A good estimate for the shear modulus of the σ phase would therefore be approximately 45 GPa. With a particle shear modulus of 45 GPa, a Poisson's ratio of 0.3, a misfit of 2.8% and a Burgers vector of 0.286 nm, the misfit strain parameter ε becomes 0.037. Therefore the critical particle diameter from coherency hardening is calculated as 3.9 nm. This small critical particle size reveals coherency hardening to be a very effective strengthening mechanism of the σ phase.

3.5. Order hardening

When a dislocation passes through an ordered precipitate an antiphase boundary (APB) is created across the slip plane with a surface energy of γ_{apb} per unit area. It is therefore energetically difficult for a single dislocation to pass through an ordered phase. Since σ has an ordered structure, order hardening is also a relevant strengthening mechanism of this phase. The γ′ phase (Ni_3Al) in nickel aluminides is also a cubic-shaped precipitate and is believed to strengthen mainly through order hardening. In γ′, two dislocations are required to pass through on the same plane to prevent leaving behind an antiphase boundary. In such materials dislocations often travel in pairs, since the energy of the antiphase boundary attracts the second dislocation. As a result, special order-hardening equations are required for such a case.

The σ phase, on the other hand, has a lattice parameter slightly more than twice that of the matrix; thus the structure of the slip planes (either {1 1 1}, {0 0 1} or {0 1 1}) is such that four dislocations with a $\frac{1}{2}\langle 0\,1\,1\rangle$ type Burgers vector would be required to pass on the same plane to prevent leaving behind an antiphase boundary. Therefore if a single dislocation begins to pass through the phase, a second dislocation would not be attracted to this same slip plane since this following dislocation would not relieve the APB energy. Consequently, dislocations in this precipitate system would not be induced to travel in pairs and special order-hardening equations are not required to determine the critical particle size from this mechanism.

The maximum order-hardening force exerted on a single dislocation occurs as it enters the particle. For a spherical particle of diameter d, this force is written [14]

$$F = \gamma_{apb} d \quad (5)$$

where γ_{apb} is the antiphase boundary energy. If order hardening were the only active mechanism the critical particle size would be

$$d_c = \frac{G_m b^2}{\gamma_{apb}} \quad (6)$$

For most ordered phases γ_{apb} lies between 0.1 and 0.3 J m^{-2}. For δ′ (Al_3Li), $\gamma_{apb} = 0.15$ J m^{-2} and for γ′ (Ni_3Al) $\gamma_{apb} = 0.18$ J m^{-2} [16]. If a value of 0.15 J m^{-2} is used as a rough estimate for the APB energy in the σ phase, a critical particle diameter of 15 nm is obtained. Consequently, the σ phase does not appear to strengthen as well from order hardening as it does from coherency hardening.

3.6. Modulus hardening

The energy of a dislocation is known to be proportional to the shear modulus of the material in which the dislocation strain field exists. The energy per unit length of an edge dislocation is written as

$$\frac{E}{L} = \frac{Gb^2}{4\pi(1-\nu)}\int_r^R \frac{dx}{x} \quad (7)$$

where r and R are the inner and outer cut-off radii for the elastic strain field, respectively, and G is the shear modulus of the material in which the strain field lies. The inner radius, defining the core, is usually given as b, the Burgers vector [17]. From this equation it is apparent that the energy of a dislocation changes as it approaches and enters a phase with a different shear modulus to that of the matrix. This change in energy results in a force felt by the dislocation.

An easily interpretable equation could not be found in the literature which described the maximum force exerted by a particle on a dislocation by the modulus-hardening mechanism. Russell and Brown [18] gave an estimate of this force, but their expression was dimensionless and depended on the outer cut-off radius of the dislocation. Thus any value could be obtained depending on what arbitrary value was used for the value of R. A simplified analysis was, therefore, performed starting from first principles. Computer simulations were performed of an edge dislocation as it approached a cubic particle with shear modulus G_p (a dislocation core radius of b was used). The dislocation was moved a distance of one Burgers vector with each step and its energy per unit length calculated. Fig. 3 is a plot of the energy of the dislocation as it approaches, enters, and then leaves a particle. A corresponding plot of the force felt by the dislocation (given by the slope of the energy curve) is also included. Although the dislocation has maximum energy at the centre of a particle, it experiences the maximum force immediately before and after it enters the particle (if the modulus of the particle were less than that of the matrix the maximum force would occur upon leaving the particle). The discontinuity observed in the force plot near the particle interface is due to the dislocation core entering the particle; no change in energy occurs during this process. This analysis revealed that although variations in the value used for the outer cut-off radius of the dislocation did slightly alter the energy of the dislocation, these variations did not measurably affect the slope of the curve or the maximum force felt by the dislocation.

From this model a plot was constructed showing the maximum force experienced by a dislocation as it entered particles of various sizes (Fig. 4). The maximum force exerted by particles with various values of shear modulus (ranging from 30 to 45 GPa) were also plotted (recall that the shear modulus of aluminium is 28 GPa). Finally, a line of constant force corresponding to Gb^2 (in aluminium) was also plotted in this figure. If the particle exerts a force on a dislocation greater than this value the dislocation will loop the particle. If the particle exerts a force less than Gb^2 the dislocation will be allowed to shear the particle. In addition, this analysis was performed for matrices with differing values of shear modulus in order to determine how G_m influences the magnitude of the maximum force, hence extending this relationship to other matrices in addition to aluminium.

With the above information, an equation was developed expressing the maximum force experienced by an edge dislocation (with Burgers vector b in a matrix

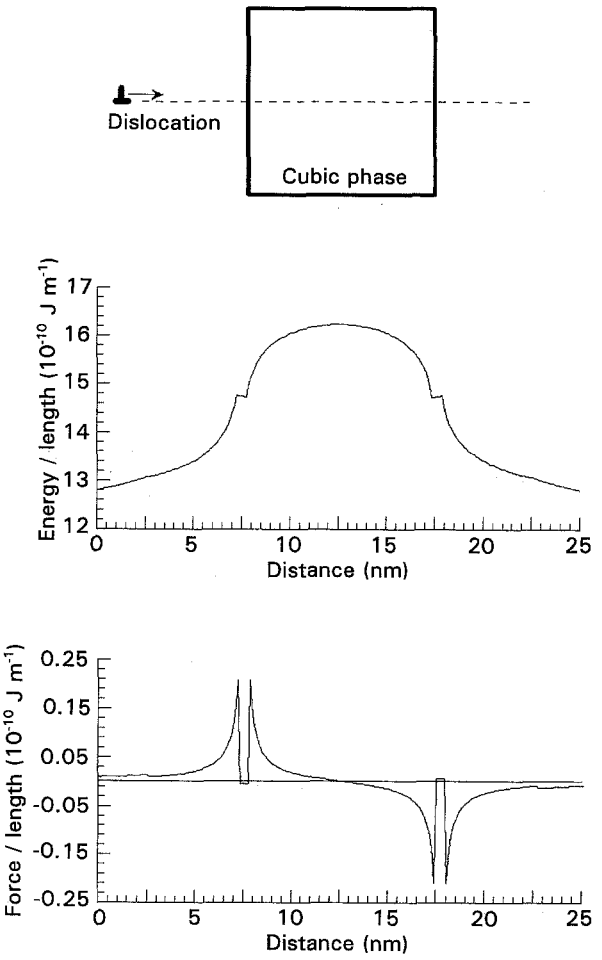

Figure 3 The energy of an edge dislocation and the force it feels as it approaches and enters a cubic particle with shear modulus of 40 GPa. The particle is 10 nm in length and is centred at a distance of 12.5 nm from the dislocation.

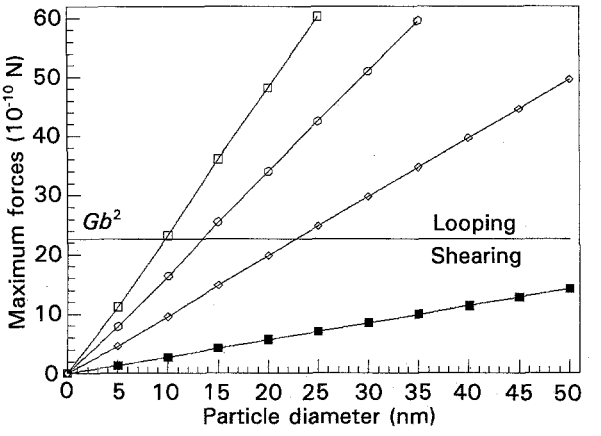

Figure 4 The maximum force exerted on an edge dislocation as it enters various-sized cubic particles with different values of shear modulus G_p: (■) 30 MPa, (◇) 35 GPa, (○) 40 GPa, (□) 45 GPa.

with shear modulus G_m) as it enters a cubic particle with edge length l and shear modulus G_p. This equation is written as

$$F = Clb\Delta G \tag{8}$$

where C is a constant with a value of 0.050 and $\Delta G = |G_p - G_m|$. Substituting Gb^2 for F yields a critical particle edge length of

$$l_c = \frac{G_m b}{C\Delta G} \tag{9}$$

Using this analysis, the critical edge length of the σ phase resulting from modulus hardening is estimated to be $l_c = 9.4$ nm (assuming $G_p = 45$ GPa).

Nembech [19], in an independent study which came to our notice following this work, derived a similar-looking equation for the force created by a spherical particle of radius r on an edge dislocation:

$$F = C_g \Delta G b^2 \left(\frac{r}{b}\right)^m \tag{10}$$

where C_g and m are constants with values roughly equal to 0.05 and 0.85, respectively. If the value of m were rounded to unity this equation would take a form similar to Equation 8.

3.7. Combined effect of the strengthening mechanisms

From the theoretical analysis performed above, coherency hardening was determined to be the dominant strengthening mechanism, followed by modulus hardening and order hardening. However, when the forces from these strengthening mechanisms were examined more closely, some were recognized to act simultaneously on a dislocation. For instance, in coherency hardening the force experienced by a dislocation increases as the dislocation approaches the interface. The maximum force, therefore, occurs directly at the interface. The maximum force from modulus hardening occurs immediately before and after a dislocation has entered the particle (as seen from Fig. 3). Thus, as a dislocation approaches the interface it simultaneously experiences forces from both elastic strains and from the difference in modulus. As a result, these forces are maximum at the interface and can be added to give a total force of

$$F = 2G_m \varepsilon bd + Clb\Delta G \tag{11}$$

This yields a critical particle diameter of

$$d_c = \frac{G_m b^2}{2G_m \varepsilon b + C\Delta G b} \tag{12}$$

From these combined mechanisms the critical diameter of the cubic σ phase is calculated as $d_c = 2.7$ nm.

A dislocation only experiences a force from order hardening when it enters the particle, so the force from order hardening could not be added to those above. However, since the maximum force from order hardening occurs immediately after the dislocation enters the particle, this force can be added to that from modulus hardening. Thus the force felt by a dislocation as it enters a particle is written

$$F = \gamma_{apb} d + Clb\Delta G \tag{13}$$

which results in a critical particle diameter of

$$d_c = \frac{G_m b^2}{\gamma_{apb} + C\Delta G b} \tag{14}$$

These forces acting together give a critical σ phase size of 6.9 nm. Thus the combined effects of coherency hardening and modulus hardening create the largest force on an approaching dislocation. The small critical particle size of 2.7 nm calculated for the σ phase suggests that this phase is a strong precipitate which would effectively repel dislocations.

3.8. Contribution of the σ phase toward the increase in yield strength

The analysis thus far has only dealt with dislocations interacting with single precipitates. However, in a real situation numerous particles are distributed randomly throughout the material and a dislocation interacts with many of these particles simultaneously. A distribution of particles, each of which exerts a force on an approaching dislocation, will increase the overall critical resolved shear stress (CRSS) (and thus the yield strength) of the alloy. Friedel [20] performed an extensive analysis of a dislocation interacting with a random array of point obstacles and expressed the increase in CRSS as

$$\Delta\tau = \frac{F_m^{3/2}}{\lambda b (2T)^{1/2}} \tag{15}$$

where F_m is the maximum force exerted by the particle (assuming $F_m < Gb^2$, the force required for looping), T is the dislocation line tension ($Gb^2/2$) and λ is the number of particles per unit area of the slip plane, written as [21]

$$\lambda = \frac{d}{2}\left(\frac{2\pi}{3f}\right)^{1/2} \tag{16}$$

where d is the particle diameter and f is the precipitate volume fraction. The increase in CRSS from particle shearing can therefore be written

$$\Delta\tau = 2.4\frac{F_m^{3/2}}{db^2}\left(\frac{f}{\pi G_m}\right)^{1/2} \tag{17}$$

If order-hardened particles are sheared by dislocations, Equations 5 and 17 can be combined to give the following expression for the increase in CRSS as a function of particle diameter d:

$$\Delta\tau_{ord} = 2.4\frac{\gamma_{apb}^{3/2}}{b^2}\left(\frac{fd}{\pi G_m}\right)^{1/2} \tag{18}$$

where γ_{apb} is the antiphase boundary energy, f the precipitate volume fraction and G_m the matrix shear modulus. Likewise the maximum force from modulus hardening (Equation 8) can be substituted into Equation 17 to obtain the following expression for the increase in CRSS from modulus hardening:

$$\Delta\tau_{mod} = 2.4(C\Delta G)^{3/2}\left(\frac{df}{\pi b G_m}\right)^{1/2} \tag{19}$$

where C has a value of 0.050. It should be noted that in a cube the edge length is similar to the diameter, so these terms can be used interchangeably.

An expression for the increase in CRSS resulting from coherency-hardened particles was given by Martin [21] to be

$$\Delta\tau_{coh} = 3.2\, G_m \varepsilon^{3/2} \left(\frac{3fd}{\pi b}\right)^{1/2} \quad (20)$$

which is very close to what would be predicted from combining Equations 3 and 17. However, experimental results by Witt and Gerold [22] indicated that this equation overestimated the strengthening by a factor of 2. Therefore a more accurate expression would instead be

$$\Delta\tau_{coh} = 1.6\, G_m \varepsilon^{3/2} \left(\frac{3fd}{\pi b}\right)^{1/2} \quad (21)$$

The increase in CRSS obtained from coherency hardening (Equation 21) and modulus hardening (Equation 19) can be combined, since the forces on a dislocation from these two mechanisms were shown to act together simultaneously. The curve representing the increase in CRSS which would result from shearing σ precipitates of various sizes is plotted in Fig. 5 (a volume fraction of 3.8% is assumed).

3.9. Orowan looping

When the size of the particle is greater than the critical diameter d_c, the particle will not be sheared. It may instead be looped by a well-known process called Orowan looping [23]. For equiaxed particles of diameter d, a good expression for the increase in CRSS resulting from this process is written as [17]

$$\Delta\tau = \frac{0.81\, G_m b}{2\pi(1-\nu)^{1/2}} \left(\frac{\ln(d/b)}{0.615d(2\pi/3f)^{1/2} - d}\right) \quad (22)$$

The increase in yield strength predicted from this equation has been demonstrated to be fairly reliable. For example, this equation accurately predicted Orowan strengthening in single Cu crystals containing Al_2O_3 and BeO particles [24]. In addition, Chaturvedi *et al.* [25] found this equation to accurately predict Orowan strengthening in a polycrystalline Co–Ni–Cr system strengthened with γ′.

The predicted increase in CRSS resulting from Orowan looping of σ precipitates of various sizes is also plotted in Fig. 5. This represents the maximum increase in yield strength from precipitate bypassing (the strengthening would be somewhat less if the particles were bypassed by cross-slip or climb, which may be the case at elevated temperature). From the plot in Fig. 5 it is readily apparent that the shearing and looping curves cross near a particle size of 2.7 nm, which is in agreement with the critical particle size calculated from the interaction of dislocations with individual cubes. This agreement lends confidence to the equations used in this analysis.

The shearing and looping curves in Fig. 5 represent the potential of the cubic σ phase for precipitate strengthening for various particle sizes. For example, it is noticed that larger phases with an edge length of 30 nm (a typically observed size) would increase the yield strength only marginally (57 MPa or 8 ksi). However, if a uniform distribution of small cubes of size 2.7 nm were produced, they could increase the yield strength by as much as 310 MPa (45 ksi), which is similar to the peak yield strength increase from the S′ phase (determined to be 270 MPa or 40 ksi [26]). σ phases with edge lengths as small as 5.0 nm have been observed in practice (Fig. 6), but a high concentration of these small phases has not been achieved thus far.

Although the σ phase has the potential for slightly better strengthening than S′, this small improvement would probably not be sufficient to encourage its use over that of S′, whose characteristics and properties have been well established over the years. However, since the interfacial energy of the σ phase appears to be quite low (modelling of the {0 0 1} interface reveals a one-to-one matching between nearest-neighbour atoms in the σ phase and in the aluminium matrix), the σ phase may exhibit a low coarsening rate. Subsequently, the greatest benefit of the σ phase may be at elevated temperatures (> 150 °C) where S′ is known to coarsen and is thus no longer effective.

In addition to the increase in yield strength, the non-shearable nature of the strong σ phase would also

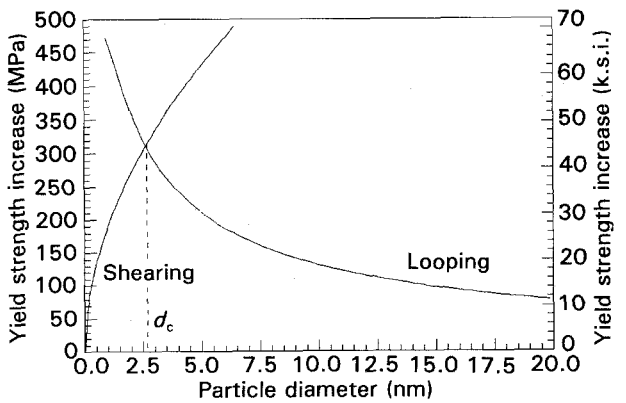

Figure 5 Increase in yield strength with particle diameter as a result of σ phase shearing and looping. This analysis gives a d_c of 2.7 nm.

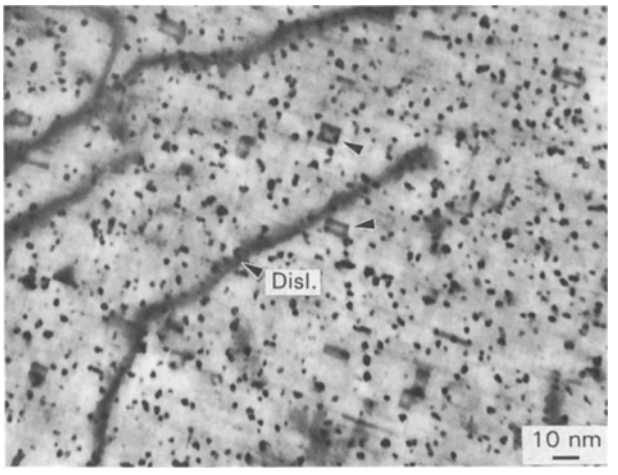

Figure 6 An example of small σ phase which had formed in the composite matrix. S′ needle ends can also be seen. **B** = [1 0 0].

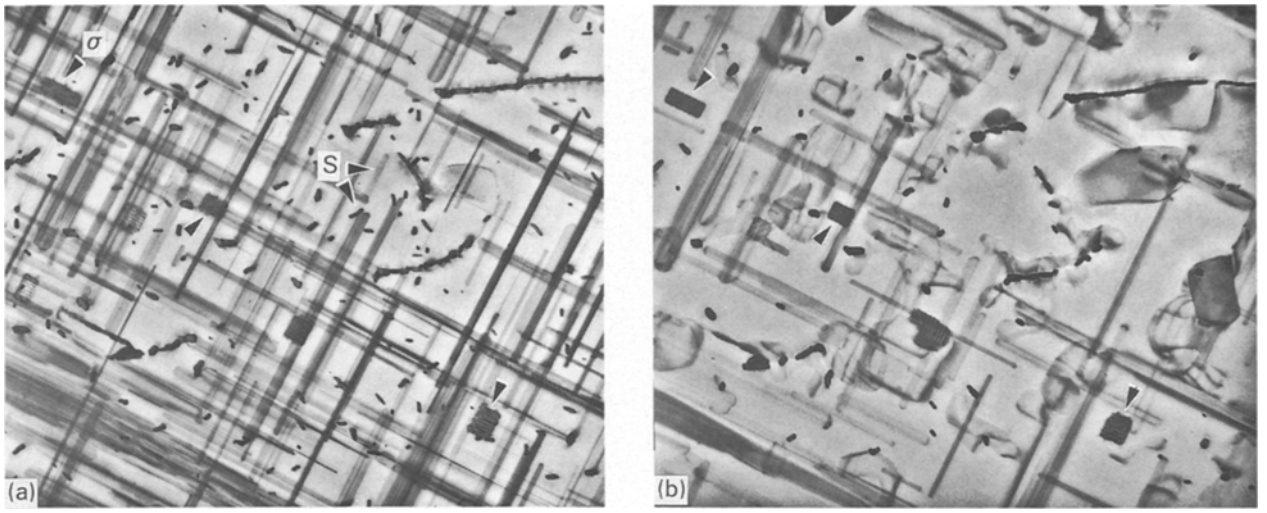

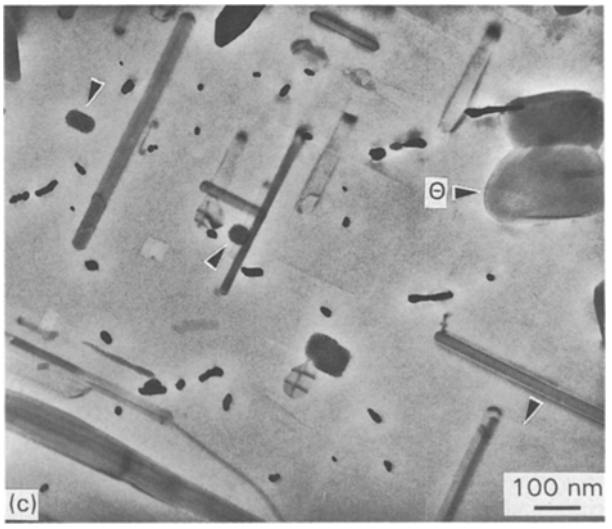

Figure 7 Unreinforced Al–4.3Cu–2 Mg–0.35Si containing S′ and σ. *In situ* hot stage at various temperatures: (a) room temperature, (b) 370 °C, (c) 410 °C.

help to improve the fracture properties of the material [27]. It is well known that weak shearable precipitates give rise to slip bands upon deformation [28]. These bands of dislocations impinge on grain boundaries and initiate cracks, resulting in low ductility and toughness values. Unshearable precipitates result in homogeneous deformation which is preferred.

3.10. Effects of high temperature on the cubic σ phase

3.10.1. Dissolution

A TEM hot stage was used to study *in situ* the effects of high temperature on the dissolution of S′ and σ in a monolithic Al–4.3Cu–2Mg–0.35Si alloy. A thermocouple attached to the heating element indicated the temperature of the specimen. The sample was held at a specific temperature for at least 10 min to ensure thermal equilibrium and prevent sample drift during photographic exposure. From Fig. 7 it is noticed that as the material was heated to a temperature of 370 °C most of the S′ phase rapidly dissolved, while the cubes retained their original size (although one cube in this figure did coarsen somewhat). As a temperature of 410 °C was reached, all but the largest S′ (with $d > 33$ nm) dissolved. At this temperature the σ phase also began to slowly dissolve, becoming more spherical and eventually disappearing after approximately 20 min. At 440 °C only large θ remained. These phases did not dissolve until a temperature of 500 °C was reached.

These results reveal that the σ phase, once nucleated, is a relatively stable phase which resists dissolution to higher temperatures than fine equilibrium S′. In addition, this analysis clearly shows that the σ phase is a precipitate which indeed dissolves during solution treatment and must, therefore, nucleate and grow after cooling.

3.10.2. Coarsening

Although it is of interest to observe the relative dissolution temperatures of the various phases, it is of more practical importance to study the coarsening behaviour of these phases during prolonged exposure at elevated temperature. Precipitate coarsening is described by the change in average particle size with increasing time. During this time the number of particles decreases so as to maintain a constant volume fraction. The driving force for coarsening is the reduction of surface energy (interfacial energy) by the overall decrease of interfacial area in the system. Therefore larger particles grow at the expense of smaller particles.

In precipitates with a relatively high value of interfacial energy the atoms are weakly bound to the interface. Therefore atoms more rapidly detach from the interface to diffuse toward larger neighbouring particles. In such instances the coarsening rate is limited by volume diffusion within the matrix, and the average particle radius varies with time according to the relationship [29, 30]

$$\langle r \rangle^3 - \langle r_0 \rangle^3 = C \frac{D_B \gamma C_B t}{kT} \qquad (23)$$

where γ is the interfacial energy, D_B is the volume diffusivity of the rate-controlling component in the

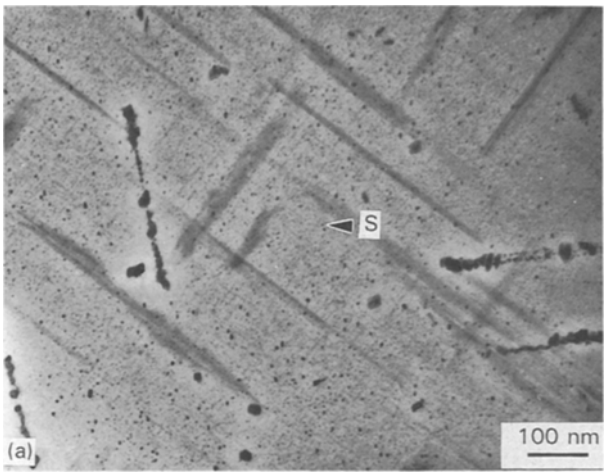

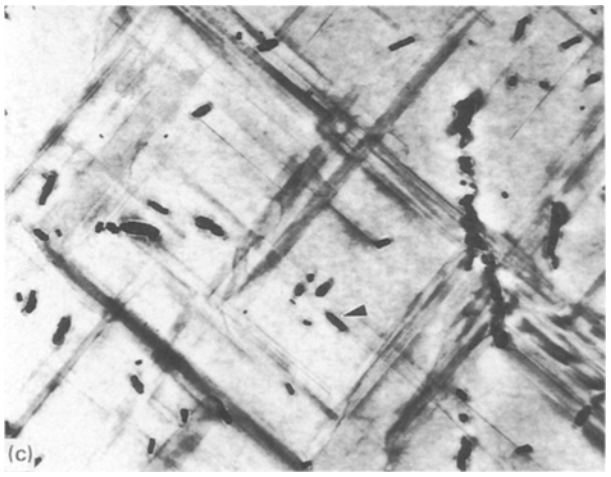

Figure 8 S′ phase after exposure to 190 °C for various periods of time: (a) 10 h, (b) 21 h, (c) 500 h. Since $\mathbf{B} = \langle 0\,0\,1 \rangle$ the S′ phase shows up as specks, which are the ends of the small needles.

matrix and C_B is its solubility in the matrix at the coarsening temperature; kT has its usual meaning. C is a constant which depends on complex statistical factors such as volume fraction and particle morphology, to name just two. This relationship shows that even in a diffusion-controlled process a low value of interfacial energy would slow down coarsening. However, if a phase has very low interfacial energy, the atoms are strongly bound to the interface and are slow to detach and migrate away. In such a case coarsening is controlled by the release rate of interfacial atoms (exchange rate of atoms across the interface) and not by diffusion. As a consequence, coarsening can take place more slowly when the interfacial energy is very low.

The coarsening effects were examined by exposing bulk materials (1 cm × 1 cm × 0.2 cm) with a previously known microstructure to elevated temperature for long periods of time. For comparison the coarsening behaviour of the S′ phase will first be addressed. Fig. 8 shows S′ after ageing a monolithic Al–4.3Cu–2Mg alloy at a temperature of 190 °C for 10, 21 and 500 h. Ageing for 10 h at 190 °C (which is near the peak ageing condition) produced fine, closely spaced S′ needles with a diameter of approximately 2.0 nm. These needles coarsened to diameters near 5.0 nm after 21 h. After exposing for 500 h the fine S′ dissolved and large, widely spaced S′ rods with a diameter greater than 20 nm formed. Dislocations would easily pass between these coarsened rods, resulting in degradation of mechanical properties. The large S′ which originally nucleated on dislocations did not appear to be affected by long-term exposure (these appear in Fig. 8 as dark lines). The S′ phase would therefore seem to have little value in applications requiring long-term exposure to temperatures of 190 °C or greater (the actual temperature limit is more like 150 °C).

A similar experiment was carried out in which material containing the σ, θ′ and S′ phases (after a T7 heat treatment) was exposed to a temperature of 190 °C for 350 h. The microstructure of the material before and after exposure is shown in Fig. 9. From these micrographs the coarsening rate of the σ phase appears to be much lower than that of the S′ and θ′ phases. Before exposure the average particle edge length was 29 nm, while during exposure the particles grew slightly to an average edge length of 33 nm (an increase of only 14%). In fact much of this growth (perhaps even all of it) occurred at the expense of the fine S′ needles and θ′ plates which were noticed to have dissolved. Therefore if the σ phase existed alone it would probably coarsen even less than shown here.

The fact that σ coarsened at the expense of S′ and θ′ implies one of two things: (i) the σ phase is more energetically stable than these other phases, or (ii) the σ phase has a lower interfacial energy. It is unlikely that σ is more energetically stable since it is only in equilibirum in high-Cu alloys (greater than 50 wt %). Consequently, this observation seems to provide evidence for the relatively low interfacial energy of the σ phase.

The coarsening behaviour of the σ phase was also investigated at a temperature of 250 °C (Fig. 9c). Once again only slight coarsening took place. At this temperature the average particle size increased from 29 to 34 nm (an increase of 19%). After exposure to a temperature of 305 °C for 350 h the cubic σ phase showed more significant signs of coarsening (Fig. 9d). The phase grew to an average particle size of 53 nm and in many cases became more spherical in shape. Thus the σ phase would not appear to be an effective strengthening phase at temperatures near 300 °C.

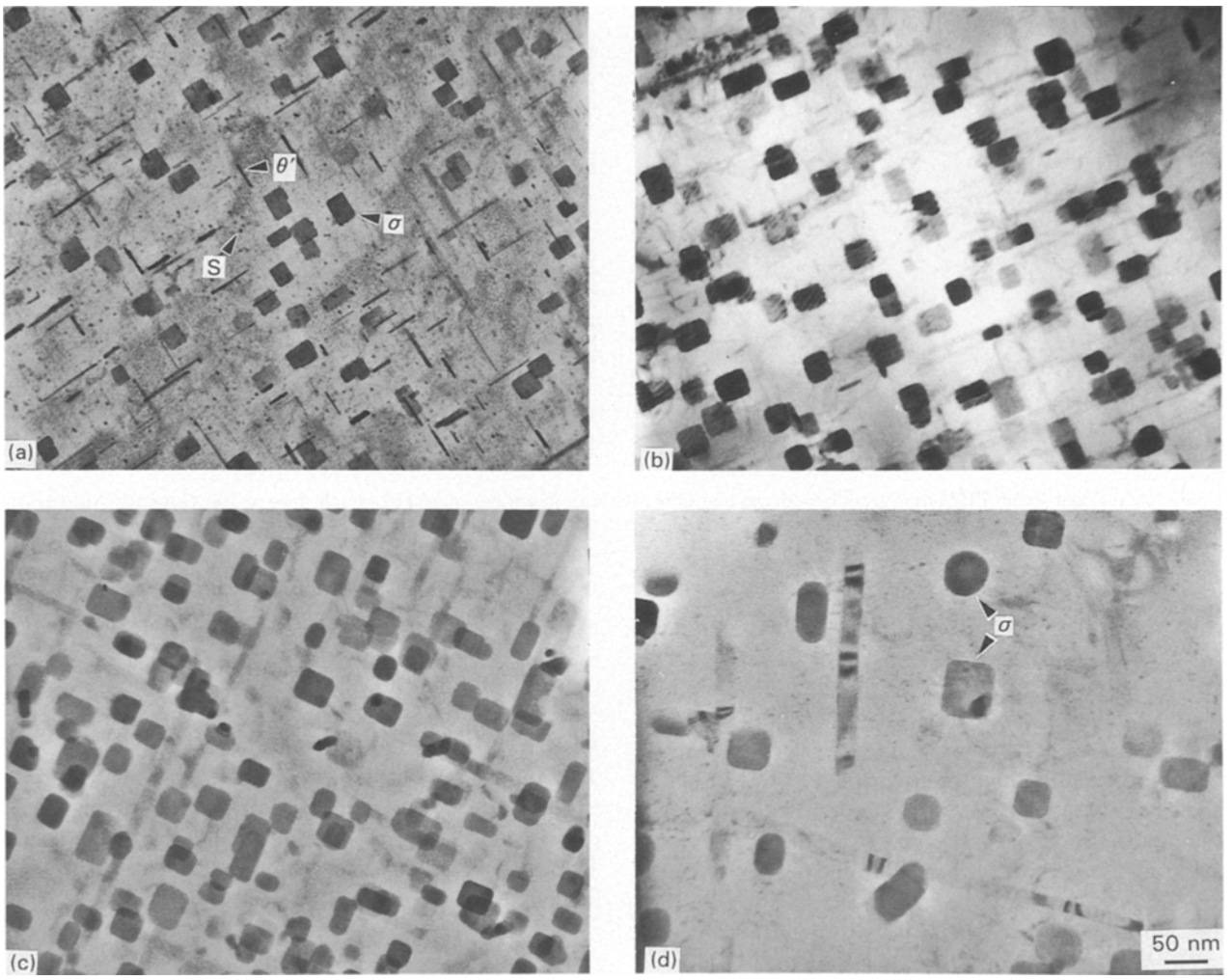

Figure 9 The coarsening behaviour of the σ, S′ and θ′ phases at elevated temperature. **B** = ⟨0 0 1⟩; (a) 190 °C/10 h, (b) 190 °C/350 h, (c) 250 °C/350 h, (d) 305 °C/350 h.

Although these results show great promise for the σ phase, it should be noted that these studies were performed on σ phases of relatively large size; the coarsening studies should more ideally be carried out on material in which the σ phase is very small and closely spaced, since this microstructure was shown to be better suited for strengthening and thus more likely to be used in practice. These studies were not possible, however, since high concentrations of small σ phase have not yet been achieved in the material.

Nevertheless, some insight into the coarsening behaviour of small σ phases can be gained by examining the general coarsening trend in a diffusion-controlled system. It is recognized from Equation 23 that if coarsening in this system is diffusion-controlled the rate of increase in particle size is larger when the particle size is small. That is

$$\frac{d\langle r\rangle}{dt} \propto \frac{C}{\langle r\rangle^2} \tag{24}$$

One can therefore surmise that even though low coarsening was observed for the larger σ particles, this does not imply that coarsening would be low for smaller particles.

The above analysis, however, is only valid if the coarsening process is diffusion-controlled, which may not be the case with the σ phase since its interfacial energy is expected to be quite low. Therefore the coarsening rate of σ may instead be interface-controlled (although there is no direct evidence to support this). If the interfacial atoms are slow to detach and diffuse into the matrix, even small closely spaced cubes may exhibit a low coarsening rate at elevated temperatures.

This investigation has demonstrated that in order to utilize the full potential of the σ phase a high concentration of small particles (near 2.7 nm) must be uniformly produced throughout an alloy. Results have shown that it is possible to form cubes to sizes as small as 5 nm, as was observed in Fig. 6. However, up to this point, attempts to generate the high nucleation rate required to produce a significant volume fraction of fine-scale σ have not been successful. In order to determine the optimum heat treatment and alloy composition which will achieve this objective, a better understanding is required as to when and how the σ phase nucleates in these alloys. Our companion paper [11] therefore focuses on the nucleation behaviour of the σ phase.

3.11. Precipitate-free zones

A potential problem with the σ phase at elevated temperature is the development of a precipitate-free

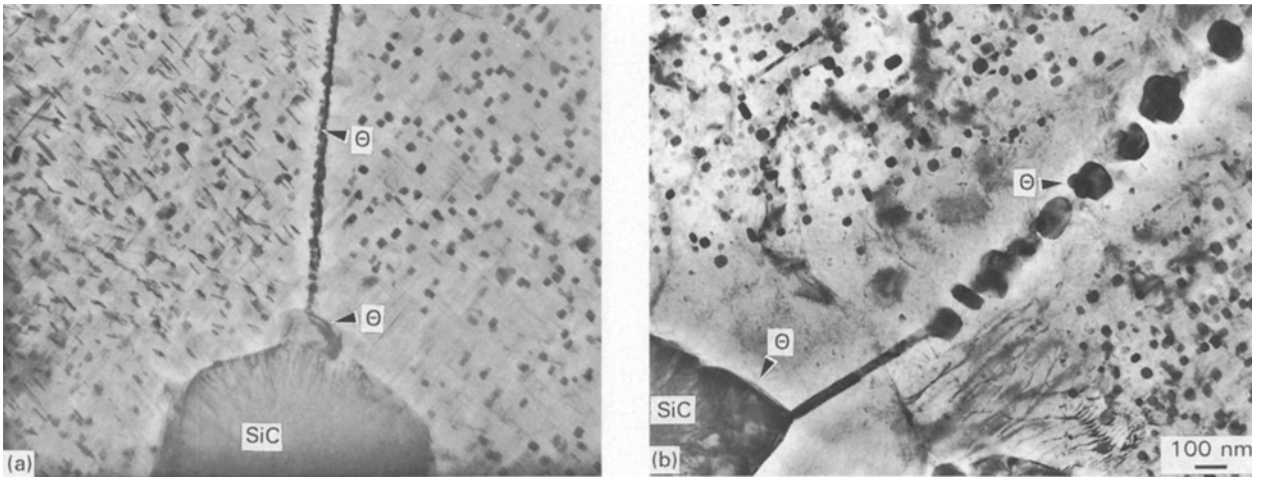

Figure 10 (a) Small 40 nm PFZs near grain boundaries and fibre interfaces in a water-quenched sample aged at 190 °C for 10 h. (b) Large 250 nm PFZs in this same material after exposing to 250 °C for 350 h.

zone (PFZ) near grain boundaries and fibre interfaces. From Fig. 10 it can be seen that as the material is held at a temperature of 250 °C for an extended period of time, large θ phases grow at the grain boundaries and fibre interfaces. The θ phase grows at the expense of nearby σ, resulting in the 0.25 μm wide PFZ. PFZs are often detrimental to mechanical properties since localized deformation occurs in such regions, often resulting in premature failure. However, the degree to which the PFZ effects the mechanical properties is unknown and will require mechanical tests to determine it.

4. Conclusions

The unusual cubic-shaped σ phase ($Al_5Cu_6Mg_2$) was investigated to determine its potential for improving the mechanical properties of an aluminium alloy at ambient and elevated temperatures. This phase was observed in volume fractions as high as 3.8%, and according to strengthening theory could increase the yield strength by as much as 310 MPa (45 ksi). However, to do so the phase would need to be uniformly distributed in sizes of 2.7 nm, a requirement which has not yet been met.

The σ phase was determined to be stable to a temperature of 410 °C, at which point it dissolved. More importantly, the σ phase resisted coarsening up to a temperature of 250 °C (due to its apparently low interfacial energy), while S′ (a phase currently heavily relied on for precipitate strengthening) was shown to coarsen significantly at temperatures of 190 °C. The S′ phase actually coarsens at temperatures as low as 150 °C, which has prevented the use of aluminium alloys and aluminium-matrix composites in many aerospace applications. The σ phase may therefore be the long-awaited coarsening resistant-phase required to extend the useful temperature range of these light materials, and it therefore deserves further investigation.

A potential problem with the σ phase at elevated temperatures, however, is the development of a precipitate-free zone near grain boundaries and whisker interfaces after long-term exposure. The apparently more stable θ phase grows on these defects at the expense of nearby σ phase.

Acknowledgements

The authors would like to extend their appreciation to General Motors Corporation for supporting this project and for fabricating the composites studied. Thanks are also due to Dr Charles P. Blankenship Jr for helpful discussions.

References

1. G. C. WEATHERLY, PhD thesis, University of Cambridge (1966).
2. R. N. WILSON, D. M. MOORE and P. J. E. FORSYTH, *J. Inst. Met.* **95** (1967) 177.
3. H. SUZUKI, M. KANNO and O. KANOH, *J. Jpn. Inst. Light Met.* **44** (1980) 1139.
4. R. D. SCHUELLER, A. K. SACHDEV and F. E. WAWNER, *Scripta Metall.* **27** (1992) 617.
5. S. SAMSON, *Acta Chem. Scand.* **3** (1949) 809.
6. L. F. MONDOLFO, "Aluminum Alloys: Structure and Properties" (Butterworth, London-Boston, 1976), p. 502.
7. R. N. WILSON and P. G. PARTRIDGE, *Acta Metall.* **13** (1965) 1321.
8. R. M. AKIN Jr, NASA Contract Report 4365 (1991) p. 55.
9. C. P. BLANKENSHIP Jr, PhD dissertation, University of Virginia (1992).
10. J. A. NOCK Jr, in "Aluminum: Properties and Physical Metallurgy", edited by J. Hatch (ASM, 1984) p. 178.
11. R. J. SCHUELLER, A. K. SACHDEV and F. E. WAWNER, *J. Mater. Sci.* **28** (1993).
12. A. J. ARDELL, *Met. Trans. A* **16A** (1985) 2131.
13. V. GEROLD and H. HABERKORN, *Phys. Status Solidi* **16** (1966) 675.
14. E. HORNBOGEN and K. H. GAHR, *Metallography* **8** (1975) 181.
15. GUILLET and LEROUX, in "Intermetallic Compounds", edited by J. H. Westbrook and R. E. Krieger (R. E. Krieger Pub. Co., New York, 1977) p. 453.
16. C. L. REYNOLDS, P. R. COUCHMAN and F. E. KARASZ, *Phil. Mag.* **34** (1976) 659.
17. J. W. MARTIN, "Micromechanisms in Particle-Hardened Alloys" (Cambridge University Press, Cambridge, UK, 1980) p. 62.
18. K. C. RUSSELL and L. M. BROWN, *Acta Metall.* **20** (1972) 969.
19. E. NEMBACH, *Phys. Status Solidi* (a) **78** (1983) 571.

20. J. FRIEDEL, "Les Dislocations" (Gauthier-Villars, Paris, 1956) p. 205.
21. J. W. MARTIN, "Micromechanisms in Particle-Hardened Alloys" (Cambridge University Press, Cambridge, UK, 1980) p. 53.
22. M. WITT and V. GEROLD, *Scripta Metall.* **3** (1969) 371.
23. E. OROWAN in Proceedings of Symposium on Internal Stresses (Institute of Metals, London, 1947) p. 451.
24. D. GOULD, PhD thesis, Oxford University (1971).
25. M. C. CHATURVEDI, D. J. LLOYD and D. W. CHUNG, *J. Mater. Sci.* **10** (1976) 373.
26. J. E. HATCH (ed.), "Aluminum: Properties and Physical Metallurgy" (ASM 1984) p. 395.
27. G. T. HAHN and A. R. ROSENFIELD, ASTM STP 432 (American Society for Testing and Materials, Philadelphia, 1968) p. 5.
28. G. LUTJERING and S. WEISSMANN, *Acta Metall.* **18** (1970) 785.
29. C. WAGNER, *Z. Elektrochem.* **65** (1961) 581.
30. I. M. LIFSHITZ and V. V. SLYOZOV, *I. Phys. Chem. Solids* **19** (1961) 35.

Received 2 February
and accepted 29 June 1993